Effect of Co_2P on Electrochemical Performance of $Li(Mn_{0.35}Co_{0.2}Fe_{0.45})PO_4/C$

H. T. Kuo,[†] T. S. Chan,[†] N. C. Bagkar,[†] G. Q. Liu,[†] R. S. Liu,*[,†] C. H. Shen,[‡] D. S. Shy,[‡] X. K. Xing,[‡] and J. M. Chen[§]

Department of Chemistry, National Taiwan University, Taipei 106, Taiwan, Synergy ScienTech Corporation, Science Tech-based Industrial Park, Hsinchu 300, Taiwan, and National Synchrotron Radiation Research Center, Hsinchu 300, Taiwan

Received: November 8, 2007; Revised Manuscript Received: April 8, 2008

In this paper, we report the synthesis of carbon coated $Li(Mn_{0.35}Co_{0.2}Fe_{0.45})PO_4$ and discuss the effect of Co_2P formation during the carbothermal reduction process, which enhances the electrochemical performance of cathode material for lithium ion batteries. It was observed that Co_2P was favorably formed in 5% H_2/Ar than in Ar atmosphere. The conductivity of $Li(Mn_{0.35}Co_{0.2}Fe_{0.45})PO_4/C$ sintered at 600−800 °C in 5% H_2/Ar is increased as the temperature is increased. The O *K*-edge X-ray absorption near edge spectrum (XANES) demonstrates that content of hole carriers is increased in $Li(Mn_{0.35}Co_{0.2}Fe_{0.45})PO_4/C$ as the amount of Co_2P increased. We also observed that the capacity of $Li(Mn_{0.35}Co_{0.2}Fe_{0.45})PO_4/C$ is increased with sintering temperature, and it exhibited a maximum capacity of 166 mAh/g at 700 °C. It was found that the enhancement in the discharge capacity of sintered $Li(Mn_{0.35}Co_{0.2}Fe_{0.45})PO_4/C$ was as a result of its higher electrical conductivity under 5% H_2/Ar atmosphere as compared with Ar atmosphere.

1. Introduction

The past decade has seen continuous efforts in the development of rechargeable lithium batteries directed toward identifying new materials suitable for the use as positive electrodes. In this regard, lithium metal oxides have been used extensively as cathode materials; for example, $LiCoO_2$, $LiNiO_2$, and $LiMn_2O_4$ are used commercially as cathode materials in rechargeable Li-ion batteries. However, these materials still have some limitations in structural stability, especially for large-scale applications in backup power systems and hybrid electric vehicles. Therefore, lithium iron phosphate ($LiFePO_4$) based on the olivine structure, exhibiting better stability, is considered an alternative cathode material for lithium ion batteries. $LiFePO_4$ offers an advantage as a cathode material in lithium ion batteries because of its high specific capacity (∼170 mAh/g) and thermal stability, it is environmentally benign, and because of its ease of fabrication.[1–3] However, the low ionic and electronic conductivity (∼10^{-9} S/cm) greatly affected the electrochemical properties of this material.[4] Hence, a lot of work has been carried out to improve and optimize the properties of $LiFePO_4$ materials which include coating with high conductivity materials on the $LiFePO_4$ [5–11] or doping with a supervalent metal ion, such as Mg^{2+}, Al^{3+}, Zr^{4+}, Nb^{5+}, and W^{6+} in $LiFePO_4$.[12] According to the supervalent doping for enhancing the conductivities of $LiFePO_4$, Molenda et al.[13,14] have observed one order increase in the electronic conductivity after the substitution of manganese for iron ($LiMn_{0.55}Fe_{0.45}PO_4$) as compared with pure $LiFePO_4$. The capacity fading during cycling is observed for the ($LiMn_{0.55}Fe_{0.45}PO_4$) compound which is also found in the $LiMn_2O_4$ system. The Jahn−Teller distortion of Mn^{3+} in those compounds has been reported which makes the structure unstable during charging and discharging leading to capacity fading.[15–17] Moreover, the similar effect corresponding to an increase in the conductivity by using the chemical substitution of Co for Fe resulting in $LiFe_xCo_{1-x}PO_4$ compositions has been reported.[18]

In order to reduce the effect of Jahn−Teller distortion of Mn^{3+} and to enhance the conductivity of $LiMn_{0.55}Fe_{0.45}PO_4$, we propose the chemical substitution of Mn^{3+} by Co^{2+} and surface coating with carbon which results in the composition of $Li(Mn_{0.35}Co_{0.2}Fe_{0.45})PO_4/C$. Wolfenstine et al.[19,20] have prepared the $LiCoPO_4$ and doped $LiCoPO_4$ using carbon-containing precursors, heated under different oxygen partial pressures (high purity argon, air, and pure oxygen) and investigated the difference in the discharged capacity for $LiCoPO_4$ samples. Interestingly, only peaks corresponding to Co_2P with no $LiCoPO_4$ peaks were exhibited when sintering is conducted under an Ar + 4% H_2 mixture after heating at 775 °C for 48 h. It suggests that the major cause of the increase in electrical conductivity of the argon sample versus the air/oxygen samples is a result of formation of metal phosphide phases. A similar result was observed for the $LiFePO_4$ system by Herle et al.[21] In any case, it is important to investigate the source (metal phosphides) responsible for the increased electrical conductivity for $LiCoPO_4$ samples heated under different sintering atmospheres. More detailed experiments are necessary, which prompted us to use the two sintering conditions to discuss the carbothermal reduction for the formation of Co_2P. The effect of varying sintering temperatures and atmosphere on Co_2P formation and the electrochemical performance of the $Li(Mn_{0.35}Co_{0.2}Fe_{0.45})PO_4/C$ have been studied systematically. We believe that the formation of Co_2P is easier during the carbothermal reduction by using (i) reductive condition (Ar + H_2 mixture gas) at lower temperature or (ii) the carbon-containing precursor or carbon-containing additives in inert (Ar) or oxidative condition (air and pure O_2) at higher temperature. The charge transfer characteristic of the $Li(Mn_{0.35}Co_{0.2}Fe_{0.45})PO_4/C$ was studied by using an electrochemical impedance spectroscopic (EIS) analysis. The influence of Co_2P on the conductivity of $Li(Mn_{0.35}Co_{0.2}Fe_{0.45})PO_4/C$ system has also been carried out using O *K*-edge X-ray absorption near edge spectrum

* To whom correspondence should be addressed. E-mail: rsliu@ntu.edu.tw.
[†] National Taiwan University.
[‡] SYNergy Scien Tech Corporation.
[§] National Synchrotron Radiation Research Center.

10.1021/jp710708r CCC: $40.75
Published on Web 06/18/2008

(XANES) analysis. The results demonstrate that the formation of residual carbon and Co_2P is greatly affected by the sintering atmosphere, and the maximum capacity was observed in the case of $Li(Mn_{0.35}Co_{0.2}Fe_{0.45})PO_4/C$ sintered at 700 °C.

2. Experimental Section

2.1. Synthesis of Cathode Materials. The $Li(Mn_{0.35}Co_{0.2}Fe_{0.45})PO_4/C$ samples were prepared via a ball milling method[22] and solid state reaction. The reactant materials MnO, FeC_2O_4, Co_3O_4, LiH_2PO_4, and 10 wt % of white sugar were weighted in stoichiometry and dispersed in acetone with zirconia balls for 18 h. After thorough drying, the powder was sintered at 600−800 °C for 8 h in 5% H_2/Ar or Ar atmosphere.

2.2. Preparation of Cathode Films and Coin Cells. Cathode materials were prepared by mixing 80 wt % active material, 10 wt % conductor (Carbon; Super P), and 10 wt % binder (polyvinylidene fluoride; PVdF) dissolved in *N*-methyl-2-pyrrolidinone (NMP). The mixture slurry was stirred in ambient for 2 h, then coated on the aluminum foil as the electronic collector. The prepared cathode was heated for 4 h at 70 °C in the oven, then cold pressed by roller with 0.04 μm thicknesses. Finally, the pressed cathode completely dried in a vacuum at 110 °C for at least 12 h to remove the traces of NMP and absorbed water in the electrode lamella. The cathode lamella was cut into circular disk with a diameter of 1 cm. The loading amount of the active materials was 10∼20 mg/cm^2. The cell consisted of a cathode and a lithium metal anode separated by a porous polyethylene film. The coin cell was assembled in the glovebox filled with the argon gas. The electrolyte was consisted of 1 M solution of $LiPF_6$ in a mixture of ethylene carbonate and dimethyl carbonate in the volume ratio of (EC:DMC = 1:1). The electrochemical testing of coin cells were performed automatically with a Maccor battery cycling system.

2.3. Characterization. The crystal structure and phase purity are characterized by X-ray diffraction (XRD) using a PANalytical X'Pert PRO diffractometer with Cu Kα radiation. To determine actual carbon content in the $Li(Mn_{0.35}Co_{0.2}Fe_{0.45})PO_4/C$ composite, elemental CHN analysis was performed on "Haraeus CHN-O Rapid" analyzer. Scanning electron microscopy (SEM) was recorded to study the morphology using Hitachi S-2400. The specific surface area was measured by a BET apparatus (TriStar 3000) in N_2 at −196 °C. The cyclic voltammetry (CV) measurements were obtained by a Cyclic Voltammeter (Digital potentiostat DP 8R and AUTOLAB model PGSTAT20) in the open circuit voltage (OCV) range from 2.00 to 4.80 V versus Li^+/Li, at 0.05 scan rates (mV/s). The conductivity measurements of bar-shape samples were carried out by using standard four-probe resistivity measurements. The electrochemical impedance spectrum (EIS) measurement was obtained by an Autolab potentiostat PGSTAT20 with frequency response analyzer (FRA). The frequency range is between 1 MHz and 0.1 Hz.

2.4. XANES Analysis. The Co *K*-edge of X-ray absorption experiments were carried out at a BL17C Wiggler beam line of the National Synchrotron Radiation Research Center (NSRRC) in Hsin-Chu, Taiwan. The electron storage ring was operated at energy of 1.5 GeV with a beam current of 300 mA. A Si(111) double-crystal monochromator was employed for energy selection with a resolution ($\Delta E/E$) around 2×10^{-4}. The data recorded at room temperature in transmission mode using gas-filled ionization chambers. The ion chambers used for measuring the incident (I_0) and transmitted (I_t) beam intensities were filled with a mixture of N_2 and H_2 gases and a mixture of N_2 and Ar gases, respectively. Energy calibration was carried out by using the first inflection point of the Co

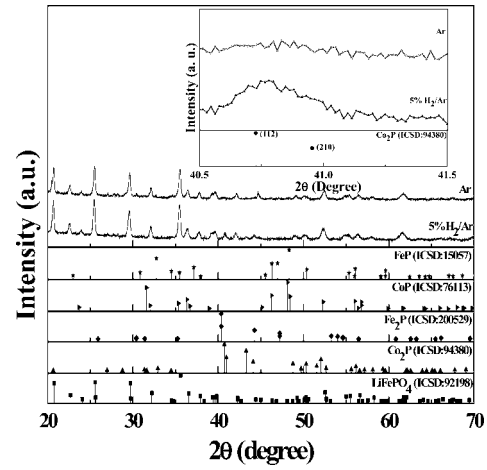

Figure 1. XRD patterns of $Li(Mn_{0.35}Co_{0.2}Fe_{0.45})PO_4/C$ sintered at 600 °C in 5% H_2/Ar and Ar atmosphere. Reflections of $LiFePO_4$ (ICSD No. 92198), Co_2P (ICSD No. 94380), Fe_2P (ICSD No. 200529), CoP (ICSD No. 76113), and FeP (ICSD No. 15057) are shown on bottom for comparison. The enlarged area from $40.5° < 2\theta < 41.5°$ is shown in the inset.

K-edge (7709 eV) absorption spectrum of Co metal foil as a reference. Reference spectra were simultaneously collected for each in situ spectrum by using V metal foils. After background subtraction, the X-ray absorption near edge structure (XANES) spectra was normalized with respect to the edge jump. The Co *L*-edge X-ray absorption measurements were performed at a 6 m high-energy spherical grating monochromator (HSGM) beam line of the NSRRC in Taiwan. The absorption spectra of Co $L_{2,3}$-edge were recorded in the X-ray sample current-yield (SC) mode in an ultrahigh vacuum chamber (10^{-9} Torr) at the 6 m HSGM. The incident photon flux (I_0) was monitored simultaneously by using a Ni mesh located after the exit slit of the monochromatic beam. All of the absorption measurements were normalized to I_0. The O *K*-edge X-ray absorption near-edge structure (XANES) measurements were performed at a 6 m HSGM beamline in NSRRC. The absorption spectra were recorded in the X-ray fluorescence-yield (FY) mode (bulk sensitive) using a microchannel plate (MCP) detector consisting of a dual set of MCPs with an electrically isolated grid mounted in front of them. The grid was set to a voltage of 100 V; the front of the MCPs was set to −2000 V, and the rear was set to −200 V. The grid bias ensured that positive ions did not enter the detector, while the MCP bias ensured that no electrons were detected. The detector was located parallel to the sample surface at a distance of ∼2 cm. Photons were incident at an angle of 45° in respect to the sample normal. The incident photon flux was monitored simultaneously by a Ni mesh located after the exit slit of the monochromator. The photon energies were calibrated with an accuracy of 0.1 eV using the O *K*-edge absorption peak at 530.1 eV of a CuO reference.

3. Results and Discussion

The XRD patterns of $Li(Mn_{0.35}Co_{0.2}Fe_{0.45})PO_4/C$ samples synthesized in different atmosphere at 600 °C are given in Figure 1. The observed peaks are in good agreement with the standard XRD pattern of $LiFePO_4$ with an olivine structure (space group: *Pnma* from ICSD file 92198). The XRD patterns of $Li(Mn_{0.35}Co_{0.2}Fe_{0.45})PO_4/C$ taken at $40.5° < 2\theta < 41.5°$ are also shown in the inset of Figure 1. It should be noted that a small amount of Co_2P phase is formed in 5% H_2/Ar atmosphere in $Li(Mn_{0.35}Co_{0.2}Fe_{0.45})PO_4/C$ sample [denoted by (112) and

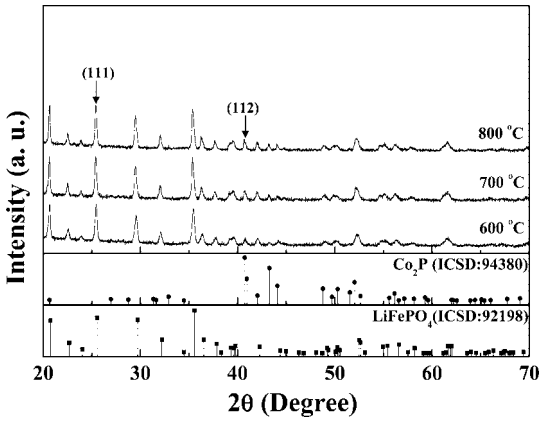

Figure 2. XRD patterns of $Li(Mn_{0.35}Co_{0.2}Fe_{0.45})PO_4/C$ sintered at 600∼800 °C in 5% H_2/Ar. Reflections of $LiFePO_4$ (ICSD No. 92198) and Co_2P (ICSD No. 94380) are shown on bottom for comparison.

(210) in Figure 1, as well as inset of Figure 1], which was not found in the sample sintered in Ar atmosphere. It should be noted that there is absence of Fe_2P, CoP and FeP phases are formed in $Li(Mn_{0.35}Co_{0.2}Fe_{0.45})PO_4/C$ sample sintered in 5% H_2/Ar and Ar atmosphere. We have also checked the paper of Nazar et al. to support our results. It suggests that FeP and Fe_2P are formed on the surface of $LiFePO_4$ via surface reduction at temperature as low as 600 °C. As the temperature is increased, the FeP will transform into Fe_2P above 600 °C by the vaporization of phosphor.[23] In addition, the elemental analysis (C, H, N) of $Li(Mn_{0.35}Co_{0.2}Fe_{0.45})PO_4/C$ sample showed the carbon content of 6.8 ± 0.1% and 3.9 ± 0.1% in 5% H_2/Ar and Ar atmosphere, respectively. The presence of Co_2P peaks as well as higher carbon content indicated the formation of Co_2P in 5% H_2/Ar, which is not observed in Ar atmosphere during the carbothermal reduction process. Therefore, the reducing atmosphere plays a major role in controlling the formation of Co_2P and the residual carbon during the sintering of samples.

The XRD patterns of $Li(Mn_{0.35}Co_{0.2}Fe_{0.45})PO_4/C$ samples synthesized in 5% H_2/Ar atmosphere at different sintering temperatures are given in Figure 2. The qualitative estimation of a particular phase is possible using intensities of XRD peak because the intensities of the diffraction lines due to one phase of the mixture depend on the proportion of that phase in the specimen.[24] In order to qualitatively estimate the Co_2P in the samples, we have normalized all XRD patterns by the maximum intensity peak of $I(111)_{LiFePO_4}$. The result shows that the amount of Co_2P phase is increased in 5% H_2/Ar atmosphere as the sintering temperature is increased. The relationship between the amount of induced Co_2P and the residual carbon content in $Li(Mn_{0.35}Co_{0.2}Fe_{0.45})PO_4/C$ samples synthesized in 5% H_2/Ar atmosphere at different sintered temperature was shown in Figure 3. It should be noticed that the reducing atmosphere at higher temperature will accelerate the carbothermal reduction process and facilitates the formation process of Co_2P. The reduced amount of residual carbon at higher temperatures may be attributed to its consumption in reducing the $Li(Mn_{0.35}Co_{0.2}Fe_{0.45})PO_4$ surface layers facilitating the formation of Co_2P. As the sintering temperature increased, the amount of Co_2P is increased which is reflected as an increase in the $I(112)_{Co_2P}/I(111)_{LiFePO_4}$ intensity ratio with a concomitant decrease in the residual carbon content.

The specific surface area as a function of temperature for $Li(Mn_{0.35}Co_{0.2}Fe_{0.45})PO_4/C$ materials sintered in 5% H_2/Ar atmosphere are shown in Figure 4. The morphology of SEM image sintered in different temperature is also shown in the inset.

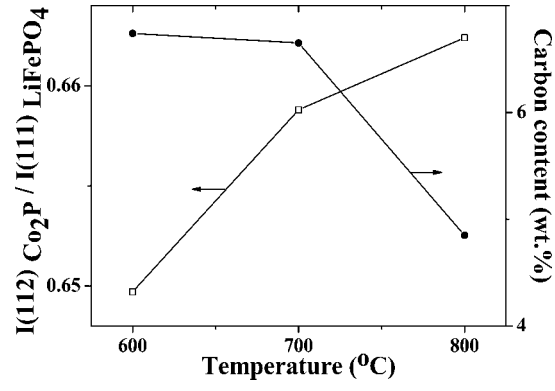

Figure 3. Intensity ratio, $I(112)_{Co_2P}/I(111)_{LiFePO_4}$, of the two peaks and carbon content plotted against the sintered temperature.

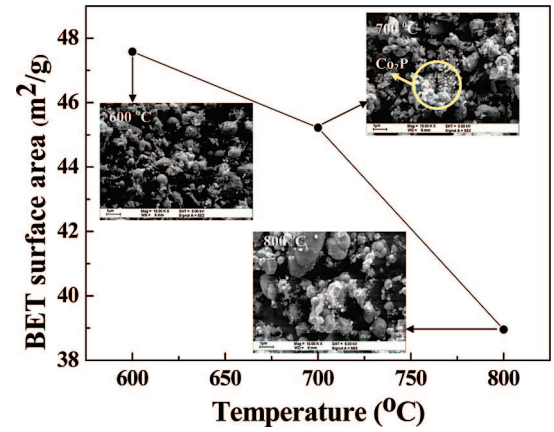

Figure 4. Specific surface area as a function temperature of $Li(Mn_{0.35}Co_{0.2}Fe_{0.45})PO_4/C$ materials sintered in 5% H_2/Ar atmosphere. The SEM image of $LiMn_{0.35}Co_{0.2}Fe_{0.45}PO_4/C$ sintered at different temperature is also show in the inset.

The specific surface area is decreased with the increasing sintering temperature. Moreover, the $Li(Mn_{0.35}Co_{0.2}Fe_{0.45})PO_4/C$ sample sintered at 600 °C showed smaller particles than prepared at higher sintering temperature (800 °C). According to SEM image, specific surface area and XRD results, we summarized the results considering several important points. First, a significant increase in particle size was observed as the sintering temperature increased. The reduced particle size is essential for electrical conductivity and for the diffusion of the lithium ions during charge/discharge processes.[6] Second, a qualitative analysis of Co_2P was performed by the direct comparison method for the normalized intensity of reflection of $Li(Mn_{0.35}Co_{0.2}Fe_{0.45})PO_4/C$ and Co_2P. Finally, the SEM image of the $Li(Mn_{0.35}Co_{0.2}Fe_{0.45})PO_4/C$ composite also showed fine spherical and white particles dispersed on the surface of the relatively large $Li(Mn_{0.35}Co_{0.2}Fe_{0.45})PO_4/C$ particles. As the sintered temperature is increased, the amount and particle size of Co_2P are also increased which confirmed that the increase in the average particle size of the $Li(Mn_{0.35}Co_{0.2}Fe_{0.45})PO_4/C$ composite was mainly due to the large particle size of the $Li(Mn_{0.35}Co_{0.2}Fe_{0.45})PO_4$ phase. The reducing atmosphere at high temperature will accelerate the carbothermal reduction process and facilitates the formation process of Co_2P.

We have performed conductivity measurements in order to investigate the effect of Co_2P formed on the conductivity of $Li(Mn_{0.35}Co_{0.2}Fe_{0.45})PO_4/C$ system. Figure 5. shows the activation energy of $Li(Mn_{0.35}Co_{0.2}Fe_{0.45})PO_4/C$ samples sintered in 5% H_2/Ar atmosphere as a function of temperature. The activation energy of $Li(Mn_{0.35}Co_{0.2}Fe_{0.45})PO_4/C$ samples sintered

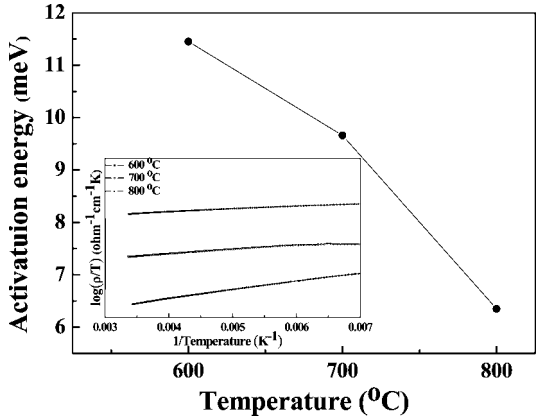

Figure 5. Calculated activation energy ($E + W$) as a function of temperature of $Li(Mn_{0.35}Co_{0.2}Fe_{0.45})PO_4/C$. The log($\rho$/T) vs 1/T plot of $Li(Mn_{0.35}Co_{0.2}Fe_{0.45})PO_4/C$ system at 600∼800 °C in 5% H_2/Ar atmosphere is also shown in the inset. The ρ is the resistivity of the bulk materials obtained from the electronic conductivity experiment.

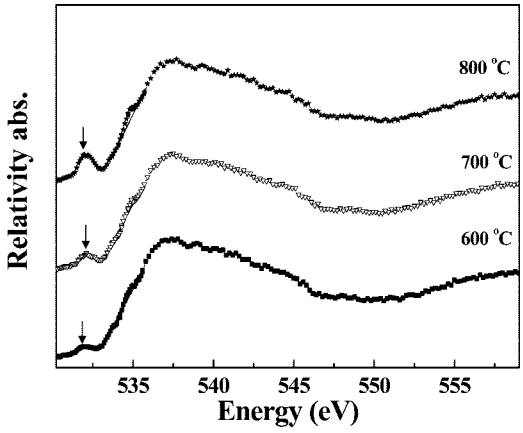

Figure 6. O *K*-edge XANES spectra of $Li(Mn_{0.35}Co_{0.2}Fe_{0.45})PO_4/C$ system at 600−800 °C in 5% H_2/Ar atmosphere. The pre-edge position of O *K* edge is shown as an arrow.

in 5% H_2/Ar atmosphere is decreased with an increase in sintering temperature. Generally, the value of activation energy is related to the band gap, and in the present case, the decrease in the activation energy can be attributed to the lowering of the band gap as a result of formation of hole carriers.[25–27] The log(ρ/T) versus 1/T plot of $Li(Mn_{0.35}Co_{0.2}Fe_{0.45})PO_4/C$ is also shown in the inset of Figure 5. It was observed that the conductivity of $Li(Mn_{0.35}Co_{0.2}Fe_{0.45})PO_4/C$ is increased with sintering temperature because of the formation of hole carriers.

In order to investigate the formation of hole carriers in $Li(Mn_{0.35}Co_{0.2}Fe_{0.45})PO_4/C$ system, we have carried out O *K*-edge XANES analysis. The O *K*-edge XANES spectra of $Li(Mn_{0.35}Co_{0.2}Fe_{0.45})PO_4/C$ samples sintered at 600−800 °C in 5% H_2/Ar atmosphere are shown in Figure 6. The spectra of O *K*-edge were recorded by measuring the X-ray fluorescence yield mode[28] at room temperature. It was observed that the most significant differences are in the pre-edge peak features as shown by the arrow in Figure 6. It is well-known that the pre-edge peaks below ∼534 eV in these spectra correspond to the transition of oxygen 1s electron to the hybridized state of the transition metal 3d and oxygen 2p orbitals, whereas the broad higher peaks above 534 eV correspond to the transitions to hybridized states of oxygen 2p and transition metal 4sp orbitals.[29] Hence, the increase in the observed pre-edge peak intensity can be explained on the basis of an enhanced hole concentration in the sample as sintering temperature is increased.

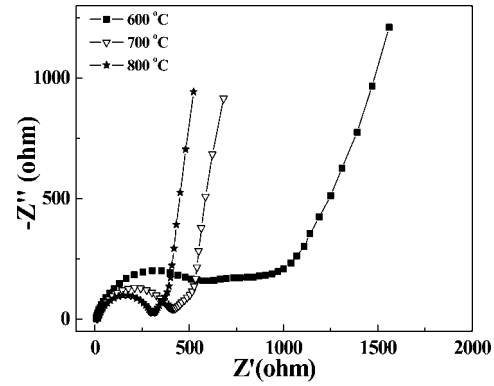

Figure 7. Nyquist plot of $Li(Mn_{0.35}Co_{0.2}Fe_{0.45})PO_4/C$ at 600∼800 °C in 5% H_2/Ar atmosphere.

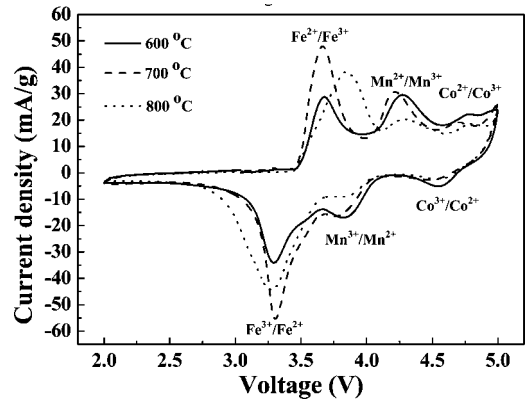

Figure 8. CV curves of $Li(Mn_{0.35}Co_{0.2}Fe_{0.45})PO_4/C$ at 600∼800 °C in 5% H_2/Ar atmosphere at scan rate 0.05 mV/s.

We have also investigated the influence of Co_2P on the charge transfer characteristic of $Li(Mn_{0.35}Co_{0.2}Fe_{0.45})PO_4/C$ using an electrochemical impedance spectroscopic (EIS) analysis. Figure 7 shows NyQuist plots of the $Li(Mn_{0.35}Co_{0.2}Fe_{0.45})PO_4/C$ sample sintered at different temperatures in 5% H_2/Ar atmosphere. The high-frequency limit shifted in the negative direction on the real axis as the temperature is increased which suggested the ohmic resistance, mainly due to Co_2P in the $Li(Mn_{0.35}Co_{0.2}Fe_{0.45})PO_4/C$ system. All plots exhibit a depressed semicircle in the high frequency region, which is attributed to the enhancement of charge-transfer process induced by Co_2P in the $Li(Mn_{0.35}Co_{0.2}Fe_{0.45})PO_4/C$ sample.

We have performed cyclic voltammetry (CV) in order to investigate the effect of Co_2P on the electrochemical properties of $Li(Mn_{0.35}Co_{0.2}Fe_{0.45})PO_4/C$ from 2.00 to 5.00 V by using a scanning rate of 0.05 mV/s. Figure 8 shows the CV plots of $Li(Mn_{0.35}Co_{0.2}Fe_{0.45})PO_4/C$ at 600−800 °C in 5% H_2/Ar atmosphere. The CV showed three clear peaks because of the redox reaction of Fe^{2+}/Fe^{3+}, Mn^{2+}/Mn^{3+}, and Co^{2+}/Co^{3+} in $Li(Mn_{0.35}Co_{0.2}Fe_{0.45})PO_4/C$. The formal redox potentials of Fe^{2+}/Fe^{3+}, Mn^{2+}/Mn^{3+}, and Co^{2+}/Co^{3+} were found to be at around 3.45, 4.0, and 4.6 V, respectively. The electrolyte used in the present investigation is found to be stable within this working potential window.[30] The oxidation peak intensities of $Fe^{2+}/Fe^{3+}$and Mn^{2+}/Mn^{3+} in $Li(Mn_{0.35}Co_{0.2}Fe_{0.45})PO_4/C$ synthesized at 700 °C were found to be higher than the sample synthesized at 800 °C. The sample synthesized at 600 °C showed the lowest values of intensities. The increased peak intensity suggests that the oxidation and reduction processes are much more strongly enhanced because of the conductivity enhancement by the formation of Co_2P at 700 °C. However, the oxidation peak intensities of Co^{2+}/Co^{3+} in $Li(Mn_{0.35}Co_{0.2}Fe_{0.45})PO_4/C$ synthe-

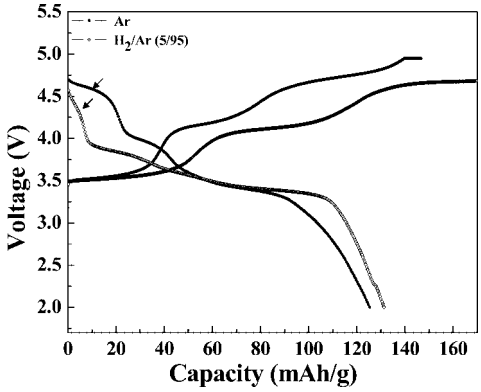

Figure 9. Discharge curves of $Li(Mn_{0.35}Co_{0.2}Fe_{0.45})PO_4/C$ at 600 °C in 5% H_2/Ar (open circles) and Ar atmosphere (solid circles) at 0.2C.

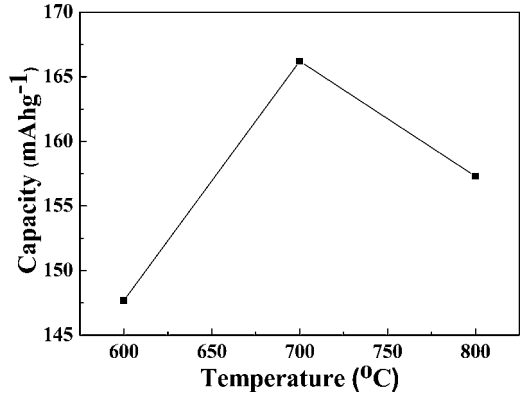

Figure 10. Capacity as a function of temperature of $Li(Mn_{0.35}Co_{0.2}Fe_{0.45})PO_4/C$ in 5% H_2/Ar atmosphere at 0.1C.

sized at 600 °C were found to be higher than the samples synthesized at 700 and 800 °C since the amount of Co in sample synthesized at 600 °C was more than in the other samples. These results are also consistent with the standard electrochemical performance reported in the literature.[31–33]

Figure 8 shows the selected galvanic profiles from 2.00 to 4.95 V at 0.2C rate of $Li(Mn_{0.35}Co_{0.2}Fe_{0.45})PO_4/C$ samples sintered at 600 °C in the 5% H_2/Ar and Ar atmosphere. As seen in Figure 9, three plateaus were observed at around 3.50, 4.10, and 4.60 V, corresponding to three redox couples present in the $Li(Mn_{0.35}Co_{0.2}Fe_{0.45})PO_4/C$ system. The plateau at 3.50 V can be attributed to Fe^{2+}/Fe^{3+} redox couple which is in good agreement with previous results. Similarly, the plateaus at 4.10 and 4.60 V can be assigned to Mn^{2+}/Mn^{3+} and Co^{2+}/Co^{3+} redox couple, respectively. It must be noted that the plateau of Co^{2+}/Co^{3+} redox couple (as shown by an arrow in Figure 9) is decreased for the sample sintered in 5% H_2/Ar system. The decrease in the plateau can be attributed to the formation of Co_2P in $Li(Mn_{0.35}Co_{0.2}Fe_{0.45})PO_4/C$ under reducing atmosphere. However, at higher sintering temperature, the Co_2P formation takes place at the expense of active cobalt ions in $Li(Mn_{0.35}Co_{0.2}Fe_{0.45})PO_4/C$ affecting the charge/discharge profile of $Li(Mn_{0.35}Co_{0.2}Fe_{0.45})PO_4/C$ for the sample sintered at 800 °C. The overall effect is increased discharge capacity (~132 mAh/g) at 600 °C in 5% H_2/Ar atmosphere than in Ar (~125 mAh/g) system. The polarization is reduced by the formation of Co_2P and more residual carbon is formed. This is most likely a result from the higher electrical conductivity due to Co_2P in the 5% H_2/Ar sample.

Figure 10 shows the capacity of $Li(Mn_{0.35}Co_{0.2}Fe_{0.45})PO_4/C$ as a function of sintering temperature. It was observed that the capacity is increased with sintering temperature until 700 °C with the maximum value of 166 mAh/g for $Li(Mn_{0.35}Co_{0.2}Fe_{0.45})PO_4/C$. However, the capacity decreases as the sintering temperature is increased further. The decrease in the capacity of $Li(Mn_{0.35}Co_{0.2}Fe_{0.45})PO_4/C$ at higher sintering temperature can be ascribed to the formation of Co_2P at the expense of active cobalt ions in $Li(Mn_{0.35}Co_{0.2}Fe_{0.45})PO_4/C$. The increase in discharge capacity is likely a result of the increase in the electronic conductivity (as supported by conductivity, cyclic voltammetric and impedance measurements) from 600 to 700 °C, associated with the conductive Co_2P on particles surfaces. Since Co_2P is electrochemically inactive and the decreased content of active cobalt ions above 700 °C together with the observed decrease in carbon content as a result of carbothermal reaction[21] are major contributing factors for the observed decrease in the capacity. The results are in good agreement with

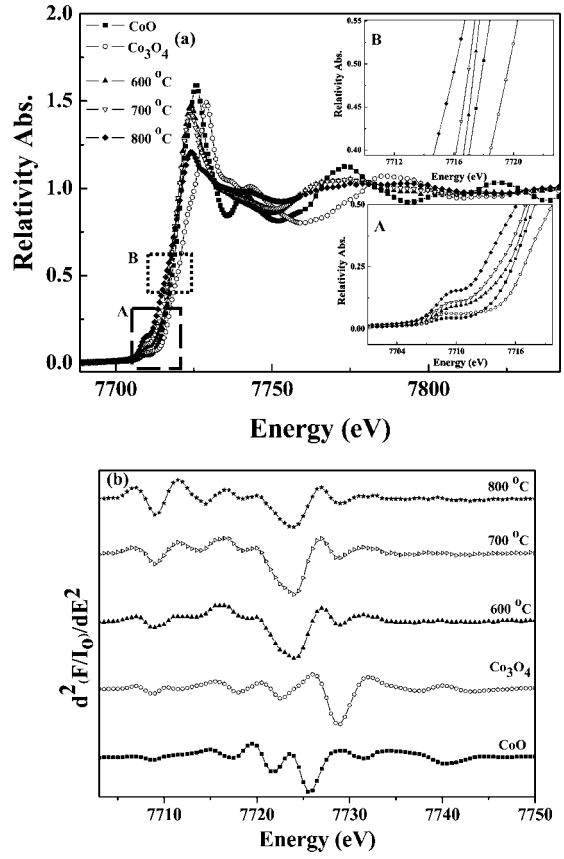

Figure 11. XANES spectra of $Li(Mn_{0.35}Co_{0.2}Fe_{0.45})PO_4/C$ sample at different temperatures at Co *K*-edge energy along with the reference materials such as CoO and Co_3O_4; pre-edge region is labeled as A and near-edge region is labeled as B, (b) second derivatives of normalized Co *K*-edge XANES spectra.

the early report by Zhang et al.[34] Thus, we have optimized the synthesis conditions in order to obtain the maximum capacity of $Li(Mn_{0.35}Co_{0.2}Fe_{0.45})PO_4/C$ by controlling the sintering temperature and reducing atmosphere (700 °C and 5% H_2/Ar). Thus, the interdependence of sintering conditions and formation of Co_2P is contributing in the overall electrochemical performance of $Li(Mn_{0.35}Co_{0.2}Fe_{0.45})PO_4/C$.

The XANES spectra at Co *K*-edge for a series of samples sintered at different temperatures along with the reference materials such as CoO and Co_3O_4 in different oxidation states are shown in Figure 11. To compare quantitatively the intensity of absorption features in various compounds, the experimental Co *K*-edge spectra were normalized using standard edge step

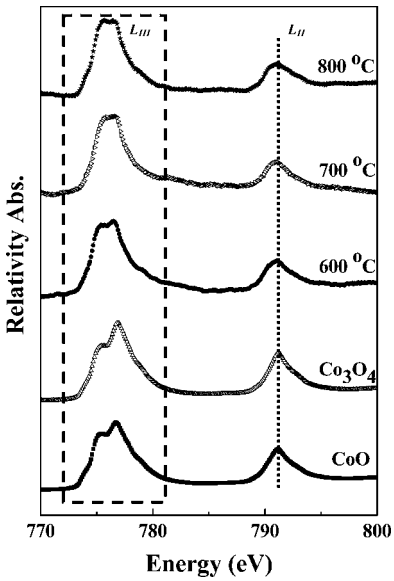

Figure 12. XANES spectra of $Li(Mn_{0.35}Co_{0.2}Fe_{0.45})PO_4/C$ at different temperatures at Co *L*-edge energy.

normalization procedure. All of the XANES spectra were reduced by background subtraction and normalized with respect to the edge jump. The absolute zero point of energy is taken with respect to the first point of inflection of the cobalt metal derivative spectrum (called E_0), which corresponds to the excitation of an inner shell electron to an empty state just above the Fermi edge of the Co metal. For each spectrum, the cobalt foil was scanned to correct for energy shift to obtain energy calibrated spectra in a consistent fashion. The pre-edge peak (labeled A in the inset) at around 7709 eV in Figure 11a is related to the 1s to 3d transition, which is electric dipole forbidden. It is well-known that this transition is dipole forbidden (symmetry forbidden) but gains intensity through the allowed electric quadrupole transition. The pre-edge peak intensity is a clear fingerprint of the symmetry change and is used to evaluate qualitatively the alteration of the cobalt local symmetry. In most of the studies, the oxidation state of cobalt is determined through the position of the absorption edge (labeled B in the inset), which shifts to lower energies with a decreasing valence state (less than divalent cation). As the temperature is increased, the formation of induced Co_2P is also increased, and the valence state of cobalt metal is shifted from high energy to low energy; the details are shown in the inset as labeled B in Figure 11a. For a better understanding and clarity of the edge features, we have shown only a smaller energy range for the XANES. Figure 11b shows the second derivative function of the Co *K*-edge for each sample with different sintering temperature. The zero crossing of the main absorption features which represents the inflection point energy was found to be from 7708.04 to 7707.94 eV for the 600 and 800 °C, respectively. Due to the formation of Co_2P phase, the curve of second derivative function for the Co *K*-edge at 600∼800 °C is shifted to lower energy. Figure 11b also shows that the zero crossing of the main absorption feature, which suggests that the local structure is similar. This is also particularly evidenced by the XANES regions.

The XAS spectra at Co *L*-edge together with the reference materials in different valence state of cobalt are shown in Figure 12. The main spectral features of the *L* edge for Co metal originate from dipole transitions of the core Co 2p level to the empty Co 3d states and are separated into two broad multiple structures by the core−hole spin−orbit interaction.[35] Both the line shape and the transition energy at the absorption edge can be used as a fingerprint to determine the chemical state and the local symmetry of the absorbing atom.[36] The spectra contain two major features because of the absorption at the Co L_{III} ($2p_{3/2}$ to 3d) and L_{II} ($2p_{1/2}$ to 3d) edges. The line shape of the Co *L*-edge is determined by the relative magnitude of the electron−electron interaction versus the bandwidth; that is, the splitting and the intensity ratio between them are determined by the interplay of crystal-field effects and electronic interactions. The chemical shift is caused by the change in the electrostatic energy at the Co site, which is driven by varying the valence states in the compounds. The absorption peak is shifted smoothly from higher energy (600 °C) to lower energy (800 °C) as the sintering temperature is increased from 600 to 800 °C as shown by the dash line in the L_{II} part. For the L_{III} part in Figure 12, the peak shape is not changed as the sintering temperature is increased from 600 to 800 °C as shown by the dash rectangle in the L_{III} part. It suggests that the crystal systems have similar crystal-field effects and electronic interactions around the cobalt metal ion.

4. Conclusion

In this paper, we demonstrate that the formation of Co_2P is favored in the 5% H_2/Ar atmosphere rather than in Ar atmosphere during the carbothermal reduction process. The presence of Co_2P in the 5% H_2/Ar system affects the charge/discharge profile and the polarization. The overall effect is an increased discharge capacity in 5% H_2/Ar atmosphere rather than in the Ar system. The measurement of the hole content in the bulk of the $Li(Mn_{0.35}Co_{0.2}Fe_{0.45})PO_4/C$ sample by O *K*-edge XANES spectra agree well with the conductivity results. The maximum capacity of 166 mAh/g was observed for the $Li(Mn_{0.35}Co_{0.2}Fe_{0.45})PO_4/C$ sample sintered at 700 °C. Moreover, the residual carbon of the samples sintered in 5% H_2/Ar atmosphere promotes the formation of Co_2P. When the sintering temperature is higher, the amount of residual carbon is decreased to induce the formation of Co_2P.

Acknowledgment. The authors would like to thank the National Science Council (Contract No. NSC 96-2120-M-002-019) for financial support.

References and Notes

(1) Tarascon, J. M.; Armand, M. *Nature* **2001**, *414*, 359.
(2) Padhi, A. K.; Nanjudaswamy, K. S.; Goodenough, J. B. *J. Electrochem. Soc.* **1997**, *144*, 1188.
(3) Thackeray, M. *Nat. Mater.* **2002**, *1*, 81.
(4) Andersson, A. S.; Thomas, J. O. *J. Power Sources* **2001**, *97*−*98*, 498.
(5) Prosini, P. P.; Zane, D.; Pasquali, M. *Electrochim. Acta* **2001**, *46*, 3517.
(6) Yamada, A.; Chung, S. C.; Hinokuma, K. *J. Electrochem. Soc.* **2001**, *148*, A224.
(7) Huang, H. Y.; n/a, S. C.; Nazar, L. F. *Electrochem. Solid State Lett.* **2001**, *4*, A170.
(8) Cho, T.-H.; Chung, H.-T. *J. Power Sources* **2004**, *133*, 272.
(9) Kwon, S. J.; Kim, C. W.; Jeong, W. T.; Lee, K. S. *J. Power Sources* **2004**, *137*, 93.
(10) Croce, F.; Epifanio, A. D.; Hassoun, J.; Deptula, A.; Olezac, T.; Scrosati, B. *Electrochem. Solid-State Lett.* **2002**, *5*, A47.
(11) Parka, K. S.; Son, J. T.; Chung, H. T.; Kim, S. J.; Lee, C. H.; Kang, K. T.; Kim, H. G. *Solid State Commun.* **2004**, *129*, 311.
(12) Chung, S. Y.; Bloking, J. T.; Chiang, Y. M. *Nat. Mater.* **2002**, *1*, 123.
(13) Molenda, J.; Ojczyk, W.; Świerczek, K.; Zając, W.; Krok, F.; Dygas, J.; Liu, R. S. *Solid State Ionics* **2006**, *177*, 2617.
(14) Ojczk, W.; Marzec, J.; Dygas, J.; Krok, F.; Liu, R. S.; Molenda, J. *Materials Science-Poland* **2006**, *24*, 103.
(15) Thackeray, M. M.; Horn, Y. S.; Kahaian, A. J.; Kelper, K. D.; Skinner, E.; Vaughey, J. T.; Hackney, S. A. *Electrochem. Solid State Lett.* **1998**, *1*, 7.

(16) Thackeray, M. M.; Johnson, C. S.; Kahaian, A. J.; Kelper, K. D.; Vaughey, J. T.; Horn, Y. S.; Hackney, S. A. *J. Power Sources* **1999**, *81*−*82*, 60.

(17) Horn, Y. S.; Hackney, S. A.; Kahaian, A. J.; Kepler, K. D.; Skinner, E.; Vaughney, J. T.; Thackeray, M. M. *J. Power Sources* **1999**, *81*−*82*, 496.

(18) Ruffo, R.; Mari, C. M.; Morazzoni, F.; Rosciano, F.; Scotti, R. *Ionics* **2007**, *13*, 287.

(19) Wolfenstine, J.; Lee, U.; Poese, B.; Allen, J. L. *J. Power Sources* **2005**, *144*, 226.

(20) Wolfenstine, J. *J. Power Sources* **2006**, *158*, 1431.

(21) Herle, P. S.; Ellils, B.; Coombs, N.; Nazar, L. F. *Nat. Mater.* **2004**, *3*, 147.

(22) Tarascon, J.-M.; Morcrette, M.; Saint, J.; Aymard, L.; Janot, R. *C. R. Chimie* **2005**, *8*, 17.

(23) Rho, Y.-H.; Nazar, L. F.; Perry, L.; Ryan, D. *J. Electrochem. Soc.* **2007**, *154*, A283.

(24) Cullity, B. D.; Stock, S. R. *Elements of X-Ray Diffraction*, 3rd ed.; 2001, 275.9.

(25) Gayathri, N.; Raychaudhuri, A. K.; Tiwary, S. K.; Gundakaram, R.; Arulraj, A.; Rao, C. N. R. *Phys. Rev. B* **1997**, *56*, 1345.

(26) Jaime, M.; Salamon, M. B.; Rubinstein, M.; Treece, R. E.; Horwitz, J. S.; Chrisey, D. B. *Phys. Rev. B* **1996**, *54*, 11914.

(27) Raffaelle, R.; Anderson, H. V.; Sparlin, D. M.; Parris, P. E. *Phys. Rev. B* **1991**, *43*, 7991.

(28) Wang, G. X.; Bewlay, S.; Needham, S. A.; Liu, H. K.; Liu, R. S.; Drozd, V. A.; Lee, J.-F.; Chen, J. M. *J. Electrochem. Soc.* **2006**, *153*, A25.

(29) Yoon, W.-S.; Chung, K. Y.; McBreen, J.; Fischer, D. A.; Yang, X.-Q. *J. Power Sources* **2006**, *163*, 234.

(30) Singhal, R.; Das, S. R.; Oviedo, O.; Tomar, M. S.; Katiyar, R. S. *J. Power Sources* **2006**, *160*, 651.

(31) Okada, S.; Sawa, S.; Egashira, M.; Yamaki, J.-I.; Tabuchi, M.; Kageyama, H.; Konichi, T.; Yoshino, A. *J. Power Sources* **2001**, *97*−*98*, 430.

(32) Lloris, J. M.; Vicente, C. P.; Tirado, J. L. *Electrochem. Solid State Lett.* **2002**, *5*, A234.

(33) Shui, J. L.; Yu, Y.; Yang, X. F.; Chen, C. H. *Electrochem. Commun.* **2006**, *8*, 1087.

(34) Zhang, S. S.; Allen, J. L.; Xu, K.; Jow, T. R. *J. Power Sources* **2005**, *147*, 234.

(35) Kang, J.-S.; Kim, J. H.; Sekiyama, A.; Kasai, S.; Suga, S.; Han, S. W.; Kim, K. H.; Muro, T.; Saitoh, Y.; Hwang, C.; Olson, C. G.; Park, B. J.; Lee, B. W.; Shim, J. H.; Park, J. H.; Min, B. I. *Phys. Rev. B* **2002**, *66*, 113105.

(36) Chen, J. G. *Surf. Sci. Rep.* **1997**, *30*, 1.

JP710708R